

Effect of Y element on atomic structure, glass forming ability, and magnetic properties of FeBC alloy

Jin-Hua Xiao(肖晋桦), Da-Wei Ding(丁大伟), Lin Li(李琳), Yi-Tao Sun(孙奕韬), Mao-Zhi Li(李茂枝), and Wei-Hua Wang(汪卫华)

Citation: Chin. Phys. B, 2024, 33 (**7**): 076101. DOI: 10.1088/1674-1056/ad3dd4
Journal homepage: http://cpb.iphy.ac.cn; http://iopscience.iop.org/cpb

What follows is a list of articles you may be interested in

Strain-tuned magnetic properties in (Ga,Fe)Sb: First-principles study

Feng-Chun Pan(潘凤春), Xue-Ling Lin(林雪玲), and Xu-Ming Wang(王旭明)
Chin. Phys. B, 2021, 30 (**9**): 096105. DOI: 10.1088/1674-1056/ac00a2

Structural, magnetic, and dielectric properties of Ni-Zn ferrite and Bi_2O_3 nanocomposites prepared by the sol-gel method

Jinmiao Han(韩晋苗), Li Sun(孙礼), Ensi Cao(曹恩思), Wentao Hao(郝文涛), Yongjia Zhang(张雍家), and Lin Ju(鞠林)
Chin. Phys. B, 2021, 30 (**9**): 096102. DOI: 10.1088/1674-1056/ac0904

Heredity of clusters in the rapidly cooling processes of Al-doped $Zr_{50}Cu_{50}$ melts and its correlation with the glass-forming ability

Dadong Wen(文大东), Yonghe Deng(邓永和), Ming Gao(高明), and Zean Tian(田泽安)
Chin. Phys. B, 2021, 30 (**7**): 076101. DOI: 10.1088/1674-1056/abea93

Ab initio molecular dynamics study on the local structures in $Ce_{70}Al_{30}$ and $La_{70}Al_{30}$ metallic glasses

F X Li(李福祥), J B Kong(孔吉波), M Z Li(李茂枝)
Chin. Phys. B, 2018, 27 (**5**): 056102. DOI: 10.1088/1674-1056/27/5/056102

Relationship between Voronoi entropy and the viscosity of $Zr_{36}Cu_{64}$ alloy melt based on molecular dynamics

Gao Wei (高伟), Feng Shi-Dong (冯士东), Zhang Shi-Liang (张世良), Qi Li (戚力), Liu Ri-Ping (刘日平)
Chin. Phys. B, 2015, 24 (**12**): 126102. DOI: 10.1088/1674-1056/24/12/126102

Effect of Y element on atomic structure, glass forming ability, and magnetic properties of FeBC alloy

Jin-Hua Xiao(肖晋桦)[1], Da-Wei Ding(丁大伟)[2,†], Lin Li(李琳)[1], Yi-Tao Sun(孙奕韬)[2], Mao-Zhi Li(李茂枝)[3], and Wei-Hua Wang(汪卫华)[2]

[1] *State Key Laboratory of Alternate Electrical Power System with Renewable Energy Sources, North China Electric Power University, Beijing* 102206, *China*

[2] *Institute of Physics, Chinese Academy of Sciences, Beijing* 100190, *China*

[3] *Department of Physics and Beijing Key Laboratory of Opto-electronic Functional Materials & Micro-nano Devices, Renmin University of China, Beijing* 100872, *China*

(Received 26 February 2024; revised manuscript received 3 April 2024; accepted manuscript online 12 April 2024)

The atomic structure of amorphous alloys plays a crucial role in determining both their glass-forming ability and magnetic properties. In this study, we investigate the influence of adding the Y element on the glass-forming ability and magnetic properties of $Fe_{86-x}Y_xB_7C_7$ ($x = 0$, 5, 10 at.%) amorphous alloys via both experiments and *ab initio* molecular dynamics simulations. Furthermore, we explore the correlation between local atomic structures and properties. Our results demonstrate that an increased Y content in the alloys leads to a higher proportion of icosahedral clusters, which can potentially enhance both glass-forming ability and thermal stability. These findings have been experimentally validated. The analysis of the electron energy density and magnetic moment of the alloy reveals that the addition of Y leads to hybridization between Y-4d and Fe-3d orbitals, resulting in a reduction in ferromagnetic coupling between Fe atoms. This subsequently reduces the magnetic moment of Fe atoms as well as the total magnetic moment of the system, which is consistent with experimental results. The results could help understand the relationship between atomic structure and magnetic property, and providing valuable insights for enhancing the performance of metallic glasses in industrial applications.

Keywords: Fe-based amorphous alloy, *ab initio* molecular dynamic simulation, glass-forming ability, magnetic properties

PACS: 61.43.Dq, 81.05.Kf, 71.15.Pd, 75.50.Kj **DOI:** 10.1088/1674-1056/ad3dd4

1. Introduction

Due to their unique atomic structure characterized by long-range disorder and short-range order, Fe-based amorphous alloys exhibit excellent magnetic and mechanical properties, which extensively contribute to their utilization as novel soft magnetic materials in electrical and electronic equipment.[1–4] Currently, significant efforts have been dedicated to enhancing the magnetic properties of Fe-based amorphous alloys through microalloying with appropriate elements and annealing processes.[5–8] However, the glass forming ability (GFA) and saturation flux density (B_s) persistently pose challenges that hinder their further industrial application.

In recent decades, there has been a remarkable advancement in the magnetic properties of Fe-based amorphous alloys, with an increase in B_s from 1.56 T (METGLAS 2605SA1) to approximately 1.7 T–1.9 T.[9–11] The primary factor contributing to this enhancement is the increased Fe content within these alloys; however, despite the increase in B_s, the GFA of the alloy is reduced due to its higher Fe content. As widely acknowledged, the excellent soft magnetic properties of Fe-based amorphous alloys are commonly attributed to the electron transfer effect between metalloid elements and Fe, while their GFA is closely associated with the atomic structure.[12–14] The limitations of experimental characterization methods for amorphous alloys make them inadequate for accurately explaining structural changes induced by microalloying, while *ab initio* molecular dynamics (AIMD) simulations have emerged as a powerful tool for investigating the intricate relationship between local atomic structures and properties in amorphous alloys.[15–19] Zhang *et al.* investigated the influence of metalloid elements (P, B, and C) on the structure and properties of Fe-based amorphous alloys through AIMD simulation.[20] Their findings revealed that the formation of covalent bonds between metalloid atoms and Fe atoms contributes to enhancing the GFA of these alloys. Ma *et al.* discovered that the addition of the Y element significantly enhances the GFA of $Co_{75}B_{25}$ alloy, as an appropriate amount of Y atoms plays a crucial role in promoting the formation of a dense atomic packing structure within the amorphous alloy.[21] However, current research primarily focuses on investigating the effects of metalloid elements on atomic and electronic structures in Fe-based amorphous alloys. The mechanism by which other transition metal elements affect their GFA, magnetic properties, and microstructure remains unclear, especially for high Fe-content amorphous alloys. In this work, we add the Y element into the $Fe_{86}B_7C_7$-based amorphous alloy and prepare $Fe_{86-x}Y_xB_7C_7$ ($x = 0$, 5, 10 at.%) amor-

†Corresponding author. E-mail: dingdawei@iphy.ac.cn

© 2024 Chinese Physical Society and IOP Publishing Ltd

phous ribbons using a single roller melt-spinning technique. Through experimental investigations combined with AIMD simulations, we systematically analyze how Y impacts the microstructure of $Fe_{86}B_7C_7$ amorphous alloy while exploring correlations among GFA, magnetic properties, and microstructure.

2. Methods

2.1. Experimental procedure

Alloys ingots with nominal compositions of $Fe_{86-x}Y_xB_7C_7$ ($x = 0$, 5, 10 at.%, hereafter denoted as Y_x) were prepared by induction-melting mixtures of pure elements of Fe (99.99 wt%), Y (99.9 wt%) and pre-alloys of Fe–B (17.84 wt% B), Fe–C (5 wt% C) in an argon atmosphere. The ingots were remelted at least five times to ensure compositional uniformity. Subsequently, the as-spun ribbons were fabricated using the single roller melt-spinning method in an argon atmosphere with a linear velocity of 40 m/s. These ribbons have a thickness of approximately 20 μm and a width of about 1 mm. The structure of the as-spun ribbons was characterized using x-ray diffraction (XRD, D8 Advance) with a Cu $K\alpha$ source. The thermodynamic parameters were determined by employing differential scanning calorimetry (DSC, NETZSCH 404 F3) under an argon flow at a heating rate of 10 K/min. The Curie temperature (T_c) was measured using a thermogravimetric analyzer (TGA, Mettler Toledo TGA/DSC 3+). Magnetic properties were measured at room temperature using a vibrating sample magnetometer (VSM) with a maximum applied field of 800 kA/m. Sample density was measured at room temperature for both experiments and simulations using the Archimedes principle.

2.2. Computational methods

AIMD simulations based on density functional theory (DFT) were performed using the Vienna *ab initio* simulation package (VASP).[21] The projected augmented wave (PAW) method was used to accurately describe the electron–ion interaction, while the generalized gradient approximation (GGA) was employed to effectively capture the exchange correlation among electrons.[22,23] All simulations were conducted in the canonical ensemble (NVT), with temperature control achieved through a Nosé–Hoover thermostat.[24] The cubic supercell containing 100 atoms with periodic boundary conditions were generated by the Monte Carlo method for alloys, and the size of the supercell was determined based on the alloy density measured at room temperature. Only Γ point was used for the Brillouin zone sampling. All alloys were equilibrated for 1500 steps (2 fs for each step) at 1600 K to remove the memory from the initial configurations. Afterwards, systems ware gradually cooled down to 1000 K and then 300 K. The cooling rates were 2×10^{14} K/s and 1×10^{14} K/s when the temperature ranged from 1600 K to 1000 K and 1000 K to 300 K, respectively. At each temperature, system volume adjusted correspondingly with zero total pressure. For accurate electron density of states (DOS) calculation, a $3\times3\times3$ k-points mesh were adopted. The DOS was calculated taking spin polarization into consideration, and the magnetic moment of the alloys was discussed based on an analysis of the DOS. Furthermore, three AIMD simulations were conducted for each alloy, resulting in highly consistent outcomes that validate both the computational approach and results.

3. Results and discussion

3.1. Amorphous nature and structural simulation

The XRD patterns of the as-spun $Fe_{86-x}Y_xB_7C_7$ ($x = 0$, 5, 10 at.%) ribbons are shown in Fig. 1(a). All samples exhibit broad diffraction peaks without any sharp peaks, indicating a completely amorphous structure of the ribbons. Furthermore, the width of these broad diffraction peaks increases with the Y content. It has been reported that there is a positive correlation between the width of the broad diffraction peak and the GFA of amorphous alloys within the same alloy system.[25] Therefore, it can be inferred that the addition of Y element enhances the GFA of $Fe_{86}B_7C_7$ alloy, and the Y_{10} alloy has the best GFA. The DSC curves of the amorphous alloy ribbons are presented in Fig. 1(b). The crystallization onset temperature is denoted as T_{x1} and T_{x2}, and the relevant thermal parameters are summarized in Table 1. Upon the addition of Y element (Y_5 and

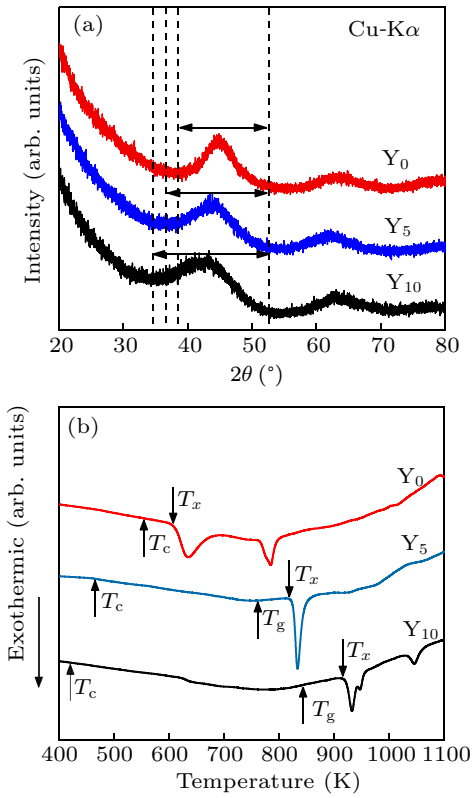


Fig. 1. (a) XRD patterns of $Fe_{86-x}Y_xB_7C_7$ amorphous ribbons, and (b) DSC curves of $Fe_{86-x}Y_xB_7C_7$ amorphous ribbons.

Table 1. Thermal parameters of $Fe_{86-x}Y_xB_7C_7$ amorphous alloys.

Amorphous alloys	T_c (K)	T_g (K)	T_{x1} (K)	T_{x2} (K)	ΔT (K)
$Fe_{86}B_7C_7$	544	–	605	722	–
$Fe_{81}Y_5B_7C_7$	461	783	817	–	37
$Fe_{76}Y_{10}B_7C_7$	415	850	915	1030	65

Y_{10} alloys), T_g is observed along with a noticeable increase in both T_{x1} and ΔT (where $\Delta T = T_{x1} - T_g$) at higher Y content, indicating enhanced GFA and thermal stability of the alloy melt.[26,27] However, T_c decreases with higher Y content, suggesting that adding the Y element impairs the thermal stability of ferromagnetic properties. Moreover, Y_5 and Y_{10} alloys exhibit an expanded temperature range for annealing ($T_g - T_c$), which is advantageous for annealing processes in industrial applications.

The influence of adding the Y element on the GFA has been investigated for $Fe_{86}B_7C_7$ amorphous alloy from an atomic structural perspective through analysis using pair distribution function (PDF), Voronoi polyhedra (VP), and bond pairs. Figure 2 shows the PDF of $Fe_{86-x}Y_xB_7C_7$ ($x = 0$, 5, 10 at.%) amorphous alloys at 1600 K and 300 K. The prominent first peak represents short-range order, while the splitting of the second peak indicates mid-range order. This is a commonly observed characteristic in amorphous alloys.[20,28] The splitting phenomenon in the second peak is commonly attributed to non-uniform connectivity among atomic clusters. Meanwhile, the liquid–glass transition may arise from a synergistic process involving enhanced local topological order and cluster formation.[16,28,29] Furthermore, a minor sub-peak is observed on the left shoulder of the first peak in the PDF curve. It is crucial to emphasize that this sub-peak does not indicate crystallization of the structure; instead, it arises due to inconsistencies in the positions of $g_{Fe-B}(r)$, $g_{Fe-C}(r)$, and $g_{Fe-Fe}(r)$.[30]

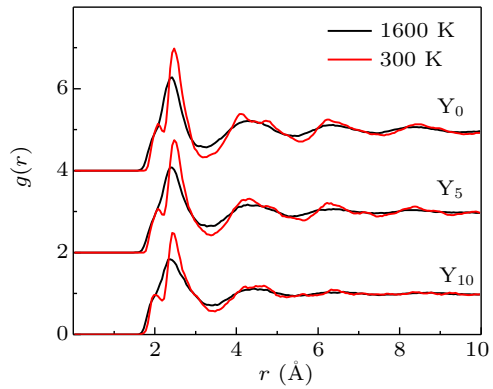


Fig. 2. PDFs of $Fe_{86-x}Y_xB_7C_7$ alloy at 1600 K and 300 K.

The partial PDFs (PPDFs) of $Fe_{86-x}Y_xB_7C_7$ ($x = 0$, 5, 10 at.%) amorphous alloys at 1600 K and 300 K are shown in Fig. 3. Considering the fact that Fe is the dominant component, only $g_{Fe-Fe}(r)$, $g_{Fe-B}(r)$, $g_{Fe-C}(r)$, and $g_{Fe-Y}(r)$ are presented. The PPDFs of $g_{Fe-B}(r)$, $g_{Fe-C}(r)$, and $g_{Fe-Y}(r)$ exhibit a pronounced first peak and a minor second peak, similar to the one observed in $g_{Fe-Fe}(r)$. The observation suggests a significant interaction between Fe atoms and Y, B, as well as C atoms, implying the formation of covalent bonds among Fe and the other three elements.[31,32] Therefore, the first peak positions of $g_{Fe-Fe}(r)$, $g_{Fe-B}(r)$, $g_{Fe-C}(r)$, and $g_{Fe-Y}(r)$ at 1600 K and 300 K are listed in Table 2. According to Table 1, it is observed that the bonding lengths of each atomic pair at 1600 K are comparatively smaller than those at 300 K. This phenomenon can primarily be attributed to the alteration in alloy magnetism. Specifically, as the alloy undergoes a transition from paramagnetic to ferromagnetic state, there is a notable reduction in the bond length of Fe atoms.[33–35] The first peak positions of $g_{Fe-B}(r)$, $g_{Fe-C}(r)$, and $g_{Fe-Y}(r)$ are compared with the sum of their atomic radii ($r_{Fe} = 1.24$ Å, $r_B = 0.90$ Å, $r_C = 0.77$ Å, $r_Y = 1.82$ Å).[2] It is evident that the distances of Fe–B, Fe–C, and Fe–Y pairs are smaller than the sum of their atomic radii ($r_{Fe-B} = 2.14$ Å, $r_{Fe-C} = 2.01$ Å, $r_{Fe-Y} = 3.06$ Å). This observation suggests the formation of covalent bonds between Fe atoms and the other three elements.[36,37] Furthermore, the increase in Y content leads to a decrease in the bond lengths of Fe–B and Fe–C, indicating an enhancement in bond strength. This phenomenon may contribute to improving the structural stability and GFA of the alloy.

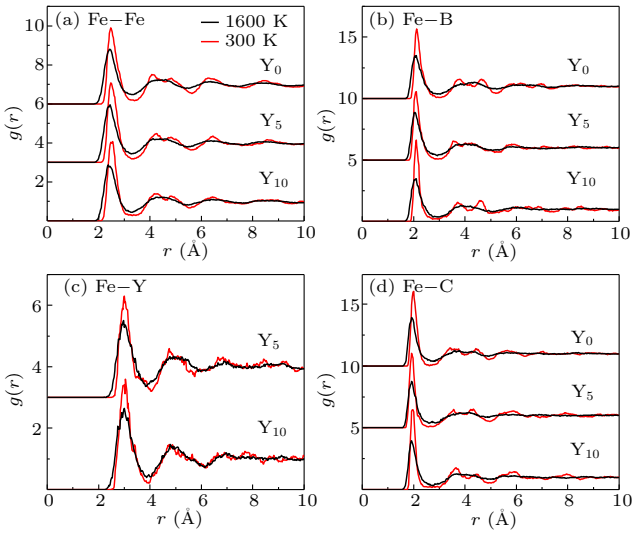


Fig. 3. PPDFs of $Fe_{86-x}Y_xB_7C_7$ alloy at 300 K: (a) Fe–Fe, (b) Fe–B, (c) Fe–Y, and (d) Fe–C.

Table 2. The positions of the first peaks for $g_{Fe-Fe}(r)$, $g_{Fe-M}(r)$, and $g_{Fe-Y}(r)$ at 1600 K and 300 K.

	$Fe_{86}B_7C_7$		$Fe_{81}Y_5B_7C_7$		$Fe_{76}Y_{10}B_7C_7$	
	160 K	300 K	1600 K	300 K	1600 K	300 K
r_{Fe-Fe}	2.45	2.48	2.45	2.48	2.45	2.48
r_{Fe-B}	2.10	2.13	2.05	2.09	2.08	2.10
r_{Fe-C}	1.93	1.99	1.92	1.93	1.93	1.95
r_{Fe-Y}	–	–	2.97	2.99	2.99	3.01

A more comprehensive investigation of the local atomic packing characteristics of $Fe_{86-x}Y_xB_7C_7$ ($x = 0$, 5, 10 at.%) amorphous alloys can be conducted using the Voronoi tessellation method. The VP index is defined as $\langle n_3, n_4, n_5, n_6 \rangle$, where n_i represents the count of i-edged faces in the Voronoi polyhedron, and the sum of n_i corresponds to the coordination number (CN) of the atom.[38] Figures 4(a)–4(c) exhibit the major VPs centered around Fe and B atoms in the three alloys. As shown in Fig. 4(a), the major Voronoi indices of Fe-centered VPs can be regarded as $\langle 0,1,10,2 \rangle$, $\langle 0,0,12,0 \rangle$, $\langle 0,2,8,4 \rangle$, $\langle 0,3,6,4 \rangle$, and $\langle 0,2,8,2 \rangle$ in all the alloys. The VP of $\langle 0,1,10,2 \rangle$, $\langle 0,2,8,2 \rangle$, and $\langle 0,0,12,0 \rangle$ is regarded as an icosahedral-like structure, $\langle 0,2,8,4 \rangle$ and $\langle 0,3,6,4 \rangle$ correspond to a deformed body-centered cubic (bcc) structure.[11,39] This suggests that the local atomic packing around Fe atoms predominantly exhibits icosahedral-like and deformed-bcc structures. From Fig. 4(b), B-centered VPs primarily consist of $\langle 0,3,6,0 \rangle$, $\langle 0,3,6,1 \rangle$, $\langle 0,4,4,0 \rangle$, and $\langle 0,2,8,0 \rangle$. Specifically, $\langle 0,3,6,0 \rangle$ and $\langle 0,3,6,1 \rangle$ correspond to the tricapped trigonal prism (TTP) and distorted TTP structure respectively, while $\langle 0,4,4,0 \rangle$ and $\langle 0,2,8,0 \rangle$ represent the Archimedean antiprism.[40] In addition to the relatively high proportion of $\langle 0,4,4,0 \rangle$ and $\langle 0,3,6,0 \rangle$, the C-entered VPs also contain other distorted TTP structures such as $\langle 0,3,5,0 \rangle$, $\langle 0,6,6,0 \rangle$, and $\langle 0,5,2,1 \rangle$.[41,42] The aforementioned observation indicates that the local atomic packing surrounding B and C atoms in the three alloys predominantly consists of trigonal prism structures. The distribution of the CNs of Fe-atoms in the three alloys is evaluated based on the results of VPs analysis, as illustrated in Fig. 4(d). The CNs of Fe atoms in the $Fe_{86}B_7C_7$ alloy are primarily 13 and 14. However, with the Y content increases, there is a gradual shift towards CNs centered around 12 and 13 for Fe atoms. This phenomenon can be attributed to the emergence of numerous small atomic clusters featuring an icosahedral structure within the amorphous alloy. The icosahedral shape of small atomic clusters, which is characterized by a central atom surrounded by 12 evenly distributed neighbors, confers relative stability and significantly enhances the GFA of alloys.[43] In contrast, the larger coordination number observed in the $Fe_{86}B_7C_7$ alloy suggests the presence of larger atomic clusters comprising more neighboring Fe atoms. Consequently, a greater number of Fe atoms participate in ferromagnetic coupling, leading to enhanced magnetic moments.[44] Therefore, while adding Y elements contributes positively to improving GFA in this alloy, it may have adverse effects on its magnetic properties.

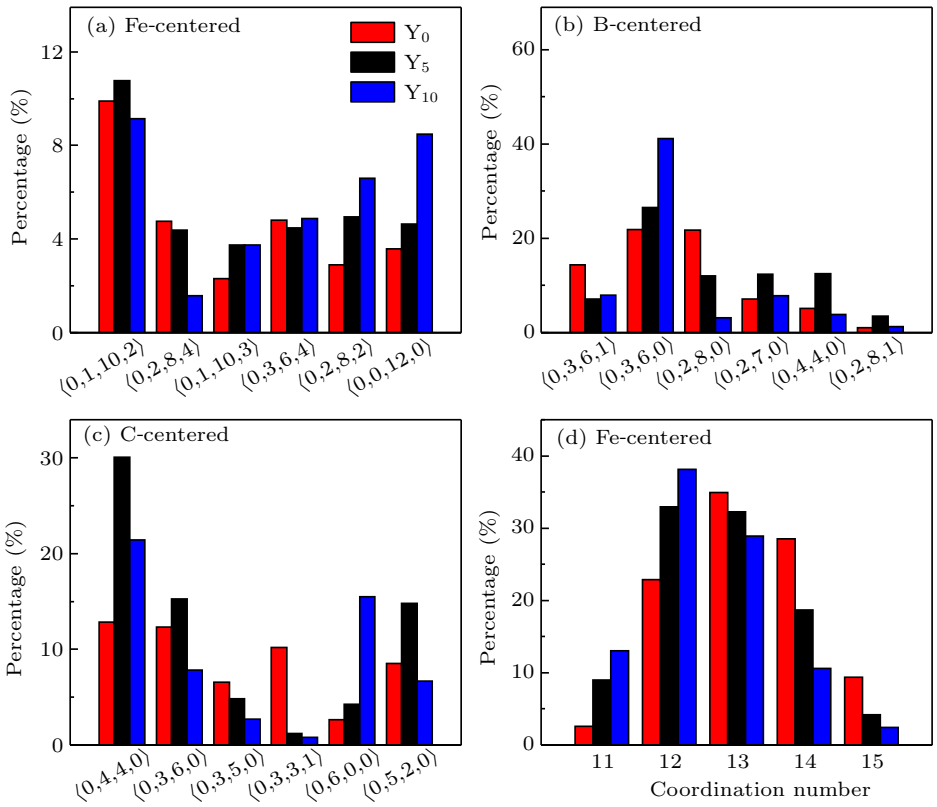


Fig. 4. (a)–(c) Fractions of major VPs centered by Fe, B, and C atoms in $Fe_{86-x}Y_xB_7C_7$ alloys, and (d) distributions of coordination number in Fe-centered clusters for all of the alloys.

The atomic clusters structure in the three alloys are further analyzed through bond pair analysis. According to Honeycutt and Andersen's theory, four indexes i, j, k, l are utilized to classify bond pairs of atomic clusters.[45] According to the nearest neighbor of $g_{ij}(r)$, if the atoms a and b form a bond, $i = 1$; otherwise, $i = 2$; j represents the number of neighboring atoms that form bonds with both a atom and b atom; k denotes the number of bonds formed by these common neighbors; l

is a special classifying index. The bond pair distributions of the three alloys are shown in Fig. 5. The alloys under investigation predominantly consist of 1541, 1551, 1431, 1441, and 1661 bond pairs. The 1541, 1551, and 1431 bond pairs exhibit associations with distorted or perfect icosahedral structure, while the 1441 and 1661 bond pairs correspond to the bcc structure.[46] The presence of abundant icosahedral structures and bcc structures is evident in all alloys. As it is known, the dense atomic packing and lack of periodicity in icosahedral structures impede crystallization nucleation, thereby significantly enhancing the GFA of all alloys.[47,48] According to the results of bond pair analysis, the proportion of bond pairs representing icosahedral structure shows an increasing trend with the increase in Y content, reaching 58.6%, 67.3%, and 71.2% for Y_0, Y_5, and Y_{10} alloys respectively. On the contrary, there is a gradual decrease in the proportion of bond pairs representing bcc structure to 24.6%, 18.3%, and 17.4% for Y_0, Y_5, and Y_{10} alloys respectively. These findings suggest that the addition of the Y element enhances the proportion of the icosahedral structure in amorphous alloy, thereby promoting its GFA.

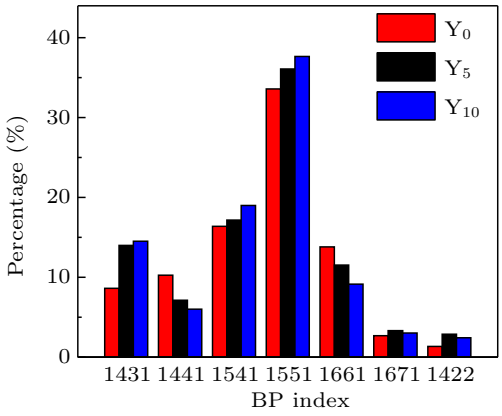


Fig. 5. Bond pairs distribution of $Fe_{86-x}Y_xB_7C_7$ alloys.

3.2. Characterization and simulation of magnetic properties

The magnetic properties of $Fe_{86-x}Y_xB_7C_7$ (x = 0, 5, 10 at.%) amorphous alloys are further investigated. The hysteresis loops of the as-spun ribbons measured by VSM are presented in Fig. 6. All the alloys exhibit the typical soft magnetic property commonly observed in amorphous alloys. The increase in Y content results in a reduction in the B_s of the alloy, indicating that the addition of Y element has an adverse effect on its magnetic properties. In order to investigate the influence mechanism of Y elements on the magnetic properties of $Fe_{86}B_7C_7$ amorphous alloy, an analysis is conducted on electronic density of states (DOS) and magnetic moment.

Figure 7 shows the total DOS of $Fe_{86-x}Y_xB_7C_7$ (x = 0, 5, 10 at.%) amorphous alloys. The DOS of all amorphous alloys exhibits a collective similarity, characterized by an asymmetric splitting between the spin-up and spin-down bands. This band splitting leads to distinct magnetic moments for spin-up and spin-down electrons, which fundamentally underlie the ferromagnetism of amorphous alloys. Furthermore, when the Fermi level falls within the gap of the spin-down band (referred to as pseudogap), an increasing depth of this gap enhances ferromagnetic properties.[49] The depth of the pseudogap in the spin-down band decreases with the Y content increases, indicating a weakening of ferromagnetism in amorphous alloy. The shapes of the partial DOS for all three amorphous alloys are very similar. As an illustration, figure 8 presents the partial DOS of the amorphous alloy $Fe_{81}Y_5B_7C_7$. The electronic states of Y_5 alloy are dominated by the 3d states of Fe atoms. Besides, there is hybridization between Fe-3d with Y-4d, B-2p, and C-2p orbital electrons, indicating that Fe atoms form bonds with these three elements. The observed hybridization suggests that Fe participates in covalent bonding with the other three elements, leading to enhanced structural stability and potentially playing a crucial role in glass formation.[42] However, this hybridization has the potential to alter electron exchange energies or orbital energy gaps, ultimately resulting in magnetically inactive atomic bonding.

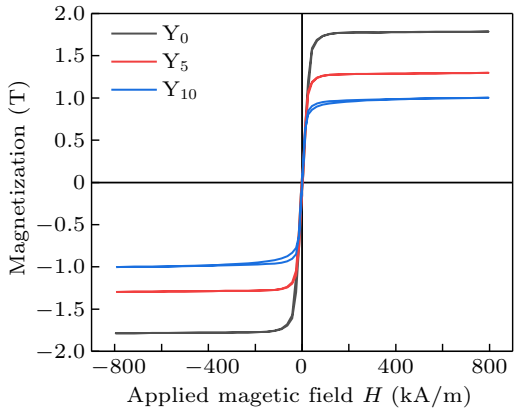


Fig. 6. Hysteresis loops of the $Fe_{86-x}Y_xB_7C_7$ (x = 0, 5, 10 at.%) amorphous alloys.

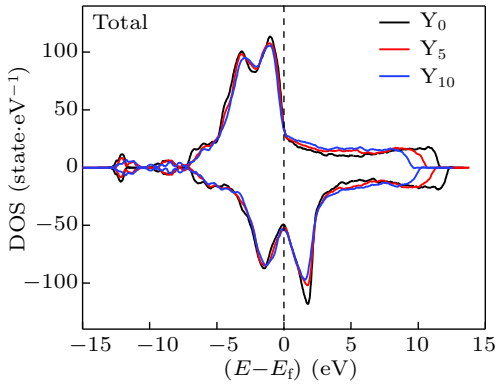


Fig. 7. The total DOS of $Fe_{86-x}Y_xB_7C_7$ alloys.

The analysis of the DOS reveals that the magnetization in all three alloys is predominantly governed by Fe-3d states, with a minor contribution from Y-4d, B-2p, and C-2p states. Therefore, Table 3 presents the average magnetic moments of

Fe as well as Y, B, and C. Negative local magnetic moments are observed for Y (-0.21 μ_B/atom), B (-0.15 μ_B/atom), and C (-0.13 μ_B/atom) due to the hybridization between Fe-3d orbitals with B-2p, C-2p, and Y-3d orbitals. The average local magnetic moment of Fe atoms in Y_0, Y_5, and Y_{10} alloys is 2.17, 2.13, and 2.10 μ_B/atom, respectively. The high magnetic moment of the Fe atom primarily arises from covalent coupling and electronegativity disparities between the Fe atom and the metalloid atoms, resulting in charge transfer from the Fe atom to these atoms.[33] Consequently, as more electrons are lost by the Fe atom, its magnetic moment increases. As the content of Y increases, there are two factors that contribute to a decrease in the magnetic moment of an Fe atom. Firstly, the adverse effects on the magnetic moment of the Fe atom caused by hybridization between Y-4d and Fe-3d orbitals. Secondly, the reduction in the number of Fe–Fe neighbors resulting from substitution of Fe by Y adversely affects ferromagnetic exchange coupling between Fe atoms, leading to a decrease in the magnetic moment of the Fe atom.[50]

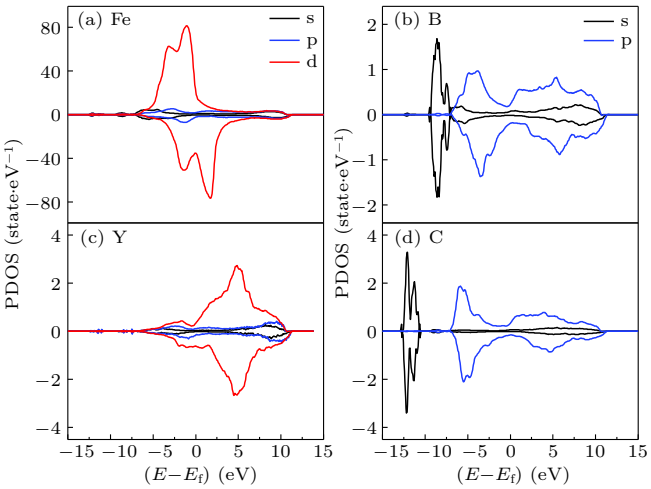


Fig. 8. The PDOS of $Fe_{81}Y_5B_7C_7$ alloys (a) Fe DOS, (b) B DOS, (c) Y DOS, and (d) C DOS.

Table 3. The magnetic moment of orbitals and total magnetic moment for the atoms in $Fe_{86-x}Y_xB_7C_7$ alloys.

Alloys	Atoms	m_s (μ_B)	m_p (μ_B)	m_d (μ_B)	M_{total} (μ_B)
$Fe_{86}B_7C_7$	Fe	–0.0099	–0.0407	2.2163	2.1657
	B	–0.0278	–0.1370	0	–0.1647
	C	–0.0148	–0.1286	0	–0.1434
$Fe_{81}Y_5B_7C_7$	Fe	–0.0079	–0.0391	2.1765	2.1295
	Y	0.0148	0.0326	0.1537	0.2011
	B	–0.0249	–0.1293	0	–0.1542
	C	–0.0136	–0.1180	0	–0.1316
$Fe_{76}Y_{10}B_7C_7$	Fe	–0.0057	–0.0366	2.0919	2.0950
	Y	0.0149	0.0358	0.1629	0.2137
	B	–0.0230	–0.1207	0	–0.1437
	C	–0.0121	–0.1041	0	–0.1161

Considering that the supercell size of all the alloys in AIMD simulation is approximately 1 nm, which is significantly smaller than the magnetic domain structure, it can be reasonably inferred that the magnetic alignment reaches saturation spontaneously. Consequently, the overall magnetic moment can be transformed into B_s using the formula

$$B_s = \mu_0 \frac{M}{V}, \tag{1}$$

where M is the calculated magnetic moment, V is the supercell volume.

The experimental results and simulated values of B_s are presented in Table 4. It can be observed that there is consistency between the variation trends of B_s in both simulated values and experimental results: an increase in Y content leads to a decrease in the B_s of amorphous alloy. Due to the presence of magnetic domain effects, achieving complete saturation becomes challenging for ribbon samples under limited magnetic fields; hence, the simulated values tend to be smaller compared to the experimental results.

Table 4. The comparison of the calculated and experimental B_s of $Fe_{86-x}Y_xB_7C_7$ alloys.

Amorphous alloys	Experimental B_s (T)	Calculated M (μ_B)	Calculated B_s (T)
$Fe_{86}B_7C_7$	1.79	181.9	1.80
$Fe_{81}Y_5B_7C_7$	1.31	166.8	1.53
$Fe_{76}Y_{10}B_7C_7$	1.04	151.7	1.29

4. Conclusion

In this paper, the atomic structure, GFA, and magnetic properties of $Fe_{86-x}Y_xB_7C_7$ ($x = 0$, 5, 10 at.%) amorphous alloys with Y addition have been investigated through experimental methods and AIMD simulations. A comprehensive analysis is conducted to elucidate the correlation mechanisms among atomic structure, GFA and magnetic properties. The main conclusions are as follows:

(i) The experimental results demonstrate that the addition of Y element enhances both the GFA and structural thermal stability of the $Fe_{86}B_7C_7$ alloy. Through analysis of the local atomic structure, it is observed that in the $Fe_{86-x}Y_xB_7C_7$ ($x = 0$, 5, 10 at.%) amorphous alloy, the local atomic packing around Fe atoms primarily exhibits an icosahedral-like and bcc structure, while B and C atoms mainly adopt a trigonal prism structure. With increasing Y content, there is a corresponding increase in the proportion of icosahedral-like structures representing clusters of Fe atom, accompanied by a decrease in bcc structure clusters. This suggests that adding Y element promotes the formation of dense atomic packing structures, thereby enhancing both structural stability and GFA.

(ii) The addition of Y element leads to a decrease in the B_s of the $Fe_{86}B_7C_7$ amorphous alloy. Analysis of electron density and magnetic moment reveals hybridization between Y-4d and Fe-3d orbitals upon Y addition. Furthermore, substitution

of certain Fe atoms with Y adversely affects ferromagnetic exchange coupling among Fe atoms. Consequently, these comprehensive effects contribute to a reduction in the overall magnetic moment exhibited by the alloy.

Data availability statement

The data that support the findings of this study are available from the corresponding author upon reasonable request.

Acknowledgements

Project supported by the National Key Research and Development Program of China (Grant No. 2021YFB2401703), the National Natural Science Foundation of China (Grant Nos. 52177005 and 51871234), and the China Postdoctoral Science Foundation (Grant No. 2022T150691).

References

[1] Wang W H, Dong C and Shek C H 2004 *Mater. Sci. Eng. R* **44** 45
[2] Takeuchi A and Inoue A 2005 *Mater. Trans. JIM* **46** 2817
[3] Suryanarayana C, Inoue A 2013 *Int. Mater. Rev.* **58** 131
[4] Wang W H 2013 *Prog. Phys.* **33** 177 (in Chinese)
[5] Ri M C, Ding D W, Sohrabi S, Sun B A and Wang W H 2018 *J. Appl. Phys.* **124** 165108
[6] Ri M C, Ding D W, Sun B A, Wang J Q, Zhu X S, Wang B B, Wang T L, Qiu Q Q, Huo L S and Wang W H 2018 *J. Non. Cryst. Solids* **495** 54
[7] Shi L and Yao K 2020 *Mater. Des.* **189** 108511
[8] Ye S, Li X, Bian X, Wang W M, Yin L and An B 2013 *J. Alloys Compd.* **562** 143
[9] Hatta S, Egami T and Graham C D 1979 *Appl. Phys. Lett.* **34** 113
[10] Wang F, Inoue A, Han Y, Kong F L, Zhu S L, Shalaan E, Al-Marzouki F and Obaid A 2017 *J. Alloys Compd.* **711** 132
[11] Wang F, Inoue A, Han Y, Zhu S L, Kong F L, Zanaeva E, Liu G D, Shalaan E, Al-Marzouki F and Obaid A 2017 *J. Alloys Compd.* **723** 376
[12] Hirata A, Hirotsu Y, Ohkubo T, Hanada T and Bengus V Z 2006 *Phys. Rev. B* **74** 214206
[13] Sheng H, Luo W, Alamgir F, Bai J and Ma E 2006 *Nature* **439** 419
[14] Poulopoulos P, Baskoutas S, Kiss L F, Bujdosó L, Kemény T, Wilhelm F, Rogalev A, Kapaklis V, Politis C, Angelakeris M and Saksl K 2008 *J. Non-Cryst. Solids* **354** 587
[15] Tian H, Zhang C, Wang L, Zhao J, Dong C, Wen B and Wang Q 2011 *J. Appl. Phys.* **109** 123520
[16] Ding J, Ma E, Asta M and Ritchie R O 2015 *Sci. Rep.* **5** 17429
[17] Yu Q, Wang X D, Lou H B, Cao Q P and Jiang J Z 2016 *Acta Mater.* **102** 116
[18] Ma H J, Wang W M, Pan S P, Cao C D and Zhang H D 2012 *Sci. Sin. Phys. Mech. Astr.* **42** 583 (in Chinese)
[19] Zhang W, Li Q and Duan H 2015 *J. Appl. Phys.* **117** 104901
[20] Ma S, Ran Y, Liang X, Jiang L, Li Y, Wang X, Yao M and Zhang W 2022 *J. Alloys Compd.* **902** 163637
[21] Kresse G and Furthmüller J 1996 *Phys. Rev. B* **54** 11169
[22] Blochl P E 1994 *Phys. Rev. B* **50** 17953
[23] Kresse G and Joubert D 1999 *Phys. Rev. B* **59** 1758
[24] Wang Y and Perdew J P 1991 *Phys. Rev. B* **44** 13298
[25] Li M X, Sun Y T, Wang C, Hu L W, Sohn S, Schroers J, Wang W H and Liu Y H 2022 *Nat. Mater.* **21** 165
[26] Suryanarayana C and Inoue A 2013 *Int. Mater. Rev.* **58** 131
[27] Inoue A 1995 *Mater. Trans. JIM* **36** 866
[28] Wu D, Li Q and Duan H 2017 *J. Non. Cryst. Solids* **461** 87
[29] Jiang J, Li Q, Duan H and Li H 2017 *Comput. Mater. Sci.* **130** 76
[30] Zhu L, Wang Y G, Cao C C and Meng Y 2017 *Chin. Phys. B* **26** 067101
[31] Wang Y, Zhang Y, Takeuchi A, Makino A, Liang Y and Kawazoe Y 2015 *Mater. Res. Express* **2** 016506
[32] Jiang Y, Jia S, Chen S, Li X, Wang L and Han X 2022 *Materials* **15** 3149
[33] Han J J, Wang W Y, Liu X J, Wang C P, Hui X D and Liu Z K 2014 *Acta Mater.* **77** 96
[34] Moroni E G, Kresse G, Hafner J and Furthmüller J 1997 *Phys. Rev. B* **56** 15629
[35] Ganesh P and Widom M 2008 *Phys. Rev. B* **77** 014205
[36] Qin J, Gu T and Yang L 2009 *J. Non-Cryst. Solids* **355** 2333
[37] Qin J, Gu T, Yang L and Bian X 2007 *Appl. Phys. Lett.* **90** 201909
[38] Finney J L 1977 *Nature* **266** 309
[39] Li M, Wang C Z, Hao S G, Kramer M J and Ho K M 2009 *Phys. Rev. B* **80** 184201
[40] Dong B S, Zhou S X, Qin J Y, Pan S P and Li Z B 2013 *Prog. Nat. Sci. Mater. Int.* **23** 216
[41] Guan P F, Fujita T, Hirata A, Liu Y H and Chen M W 2012 *Phys. Rev. Lett.* **108** 175501
[42] Ma H J, Shen K C, Pan S P, Zhao J, Qin J Y, Kim K B and Wang W M 2015 *J. Non-Cryst. Solids* **425** 67
[43] Wang Y, Takeuchi A, Makino A, Liang Y and Kawazoe Y 2015 *J. Appl. Phys.* **117** 17B705
[44] Lu L J, Guo Y M, Li X and Zhang T 2022 *J. Alloys Compd.* **904** 164101
[45] Honeycutt J D and Andersen H C 1987 *J. Phys. Chem.* **91** 4950
[46] Li X, Zuo L, Zhang X and Zhang T 2018 *J. Phys. Chem. C* **122** 28613
[47] Ma S, Hao W Y, Wang X D, Zhang W and Yao M 2022 *Acta Phys. Sin.* **71** 228102 (in Chinese)
[48] Sun C, Xu H, Meng Y, Wang X, Han M, Qiao B, Wang Y and Zhang T 2022 *Materials* **15** 8416
[49] Wang H, Hu T and Zhang T 2013 *Physica B* **411** 161
[50] Tian H, Zhang C, Zhao J, Dong C, Wen B and Wang Q 2012 *Physica B* **407** 250